Available online at www.sciencedirect.com
SCIENCE DIRECT®
Ocean Engineering 31 (2004) 21–42
OCEAN ENGINEERING
www.elsevier.com/locate/oceaneng

Wave-induced seabed response analysis by radial point interpolation meshless method

J.G. Wang [a,*], Bingyin Zhang [b], T. Nogami [c]

[a] *Tropical Marine Science Institute, National University of Singapore, 10 Kent Ridge Crescent, 119260 Singapore*
[b] *Department of Hydraulic Engineering, Tsinghua University, Beijing 100084, China*
[c] *Department of Civil Engineering, National University of Singapore, 10 Kent Ridge Crescent, 119260 Singapore*

Received 14 November 2002; received in revised form 2 May 2003; accepted 23 May 2003

Abstract

Wave-induced transient response of seabeds is numerically analyzed through a radial point interpolation meshless method (radial PIM). The Biot's consolidation theory is employed and incorporated with virtual boundary conditions to describe this wave-induced transient response of the seabed. Displacement and pore water pressure are spatially discretized by the radial PIM with the same shape function. Compactly supported basis functions are proposed to obtain a banded system equation. Because the radial PIM passes through all nodal points within an influence domain, essential boundary conditions as well as virtual boundary conditions can be easily implemented at local level. Fully implicit integration scheme is used in time domain to avoid spurious ripple effect. The proposed algorithm is assessed through the comparison of numerical results with closed-form solution or finite element solutions.

Keywords: Meshless method; Radial basis functions; Compactly supported basis; Consolidation process; Wave loads; Pore water pressure; Periodic conditions

1. Introduction

The wave-induced transient response of seabed soils is an important topic in coastal engineering, offshore structures, and wave propagation in geological medium

* Corresponding author. Tel.: +65-6874-6591; fax: +65-6779-1635.
E-mail address: tmswjg@nus.edu.sg (J.G. Wang).

0029-8018/$ - see front matter
doi:10.1016/S0029-8018(03)00112-4

(Sumer et al., 2001). Seabed soils are generally modeled as two-phase media comprising deformable soil skeleton and pore water. A water-filled porous medium theory proposed by Biot (1941) is successful in analyzing this transient response (Madsen, 1978; Okusa, 1985; Hsu and Jeng, 1994). This transient response problem can be solved in either frequency domain (Jeng and Lin, 1996) or time domain (Karim et al., 2002). They used finite element method (FEM) and finite difference method (FDM) to discretize spatial variables (Mase et al., 1994). FEM or FDM is successful in most transient responses of the seabed. However, for those problems with heavy element distortion such as large deformation and moving boundary problems, FEM confronts difficulty in remeshing their problem domains when adaptive computation is carried out. For those problems, the numerical methods, which do not depend on any element such as meshless methods, have salient advantages.

Remarkable progress has been made for the development and application of meshless methods in recent years. For example, element-free Galerkin method, based on Galerkin weak forms for energy integration and moving least square method (MLS) in constructing shape functions over a cluster of scattered nodes, has been widely applied to various problems such as solid mechanics (Belytschko et al., 1996) and deformable multiphase porous media (Modaressi and Aubert, 1998; Karim et al., 2002). Regarding a continuum problem as a discrete system, reproducing kernel particle method (Liew et al., 1995) introduced a correction function and a window function to improve the smoothed particle hydrodynamic method. This kernel particle method is successful in the simulation of impact, blasting and elastoplastic deformation problems (Liew et al., 2002). Because the shape functions of the MLS do not have delta function properties at nodes and node index instead of nodal value participates the computation in the system equation, special effort has to be made to implement essential boundary conditions (Belytschko et al., 1996). A radial point interpolation meshless method (radial PIM) was proposed to avoid this disadvantage of MLS (Wang and Liu, 2002a). This radial PIM has the shape functions with delta function properties. Another famous merit of the radial PIM is that radial basis functions map multi-dimensional spaces into one-dimensional space. In one-dimensional space, basis functions are easily chosen to satisfy the smoothness of the interpolation and to avoid the singularity in constructing shape functions. Further, the radial PIM employed mixture of radial and polynomial basis functions to achieve the accuracy of polynomials in interpolation.

Radial basis functions have been successfully applied to partial differential equations in solid mechanics and fluid mechanics. The first solution was obtained by Kansa (1990) for computational hydrodynamics. His algorithm is similar to FDM, however the sensitivity of solutions to nodal distributions within a problem domain is significantly reduced. This property significantly improves the robustness of the meshless methods based on radial basis functions. Collocation method based on radial basis functions, as a truly meshless method, was developed as an effective meshless method (Fasshauer, 1997). The collocation method brings two demerits into meshless methods: the boundary conditions at internal and external bound-

aries are not easily treated. Current treatments are almost the same as FDM. Furthermore, higher order derivatives of shape functions are required compared to the weak form. This requirement is not easy to be satisfied in practice, because higher smoothness will make the shape functions complicated. The meshless methods based on the weak form like Galerkin method can avoid above two demerits, although background mesh is required for integration. The radial PIM which is based on weak form has been successful in solid mechanics problems (Wang and Liu, 2002a) and consolidation problems (Wang et al., 2002). The shape parameters in multiquadric and exponential basis functions were also studied for domain problems (Wang and Liu, 2002b) and boundary problems (Xie et al., 2003) in solid mechanics.

This paper will study the wave-induced transient response of a seabed using radial PIM with a compactly supported radial basis function. This algorithm has advantages over those meshless methods that use the MLS to construct their shape functions. First, wave-induced water loading can be easily implemented. When water wave propagates over a seabed, a cyclic water pressure will exert on the seabed surface, thus causing pore water in the seabed to flow and seabed to deform. This transient fluctuation of pore water pressure generates the transient reduction of effective stresses. The seabed may lose its strength momentarily during a cyclic wave (Sakai et al., 1992). Second, virtual boundary conditions are easily treated within the framework of the current algorithm. Virtual boundaries refer to these boundaries due to cut-off when only one-wave or longer domain is used as the computational domain. Because wave is usually periodic and the seabed is layered, the transient response of the seabed is usually periodic. For sinusoidal waves, these virtual boundaries are periodic. Thus, the virtual boundaries are also called periodic conditions in this paper. Karim et al. (2002) proposed a revised variational principle to treat these periodic boundaries. Such a treatment will enlarge the size of the global stiffness equation and the stiffness matrix obtained is not symmetric. This makes the solution process consume more CPU time. Jeng and Lin (1996) adopted periodic conditions in their numerical simulation of water wave–soil interaction problems through FEM algorithm. The current algorithm in this paper introduces periodic boundary conditions through only assigning the same unknowns. The implementation can be achieved at the Gaussian integration process, which is much simpler and more efficient. Third, the water over the seabed and the pore water in the seabed will interact each other, affecting wave train and wave dispersion equation within water domain. In order to take the interaction into account, a solver for the transient response of the porous medium is necessary. The current algorithm is designed as a porous solver for the coupling of the wave–seabed interaction problem.

The current algorithm is based on the Biot's consolidation theory under wave loading. For simplification, acceleration is temporarily omitted, which is reasonable for long period wave. This paper is organized as follows: the Biot's consolidation theory is expressed through six physical concepts in Section 2. Such an expression can easily take the compressibility of pore fluid and the anisotropy of permeability. Furthermore, the anisotropy of soil skeleton can be included in the constitutive

laws of soils. As a preliminary study, our effort is limited to only linear elastic seabed. A Galerkin weak form is developed through a global equilibrium at each time step. Section 3 states the discretization of the weak form. The radial PIM technique is employed to discretize two spatial variables, displacement and excess pore pressure, with the same shape functions. For time domain, a fully implicit scheme is used to avoid spurious ripple effect. Section 4 discusses the numerical implementation for periodic boundary condition and wave load condition. Section 5 briefs the radial point interpolation method and compactly supported radial basis functions. As an extension of the Wendland's compactly supported radial basis functions, the current radial PIM includes both polynomial and radial basis functions. Section 6 studies a numerical example to assess the current algorithm. The numerical results obtained by the current algorithm are compared with Madsen's and Hsu and Jeng's closed-form solutions (Madsen, 1978; Hsu and Jeng, 1994) or FEM results. Finally, several key parameters such as influence domain size, time step size, and radial basis functions are studied to check its accuracy and efficiency.

2. Biot's consolidation theory and its weak form

This section describes a wave-induced seabed response problem as shown in Fig. 1. The seabed is composed of pore water and porous soil skeleton. These two phases interact with each other under wave loading. For the interaction of pore water and porous skeleton, Biot's consolidation theory (Biot, 1941) provides a good macro-level description. If acceleration is not considered, this theory is composed of six physical concepts as following:

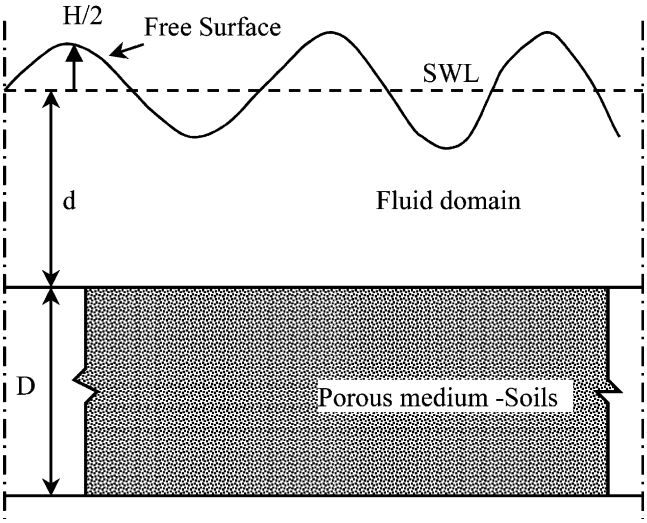

Fig. 1. Wave-induced transient response of seabed.

- Equilibrium equation of soil–water mixture

$$\frac{\partial \sigma_{ij}}{\partial x_j} + b_i = 0 \qquad \text{in V} \tag{1}$$

Or its incremental form in time interval $[t, t+\Delta t]$

$$\frac{\partial \Delta\sigma_{ij}}{\partial x_j} + \Delta b_i = -\left(\frac{\partial \sigma^t_{ij}}{\partial x_j} + b^t_i\right) \qquad \text{in V} \tag{2}$$

- Relationship of displacement and strain for soil skeleton

$$\varepsilon_{ij} = \frac{1}{2}\left(\frac{\partial u_i}{\partial x_j} + \frac{\partial u_j}{\partial x_i}\right) \qquad \text{in V} \tag{3}$$

- Constitutive law of soil skeleton in differential form

$$\mathrm{d}\sigma'_{ij} = D_{ijkl}\mathrm{d}\varepsilon_{kl} \qquad \text{in V} \tag{4}$$

- Darcy's seepage law for pore water flow

$$q_i = -\frac{K_{ij}}{\gamma_w}\frac{\partial P}{\partial x_j} \qquad \text{in V} \tag{5}$$

- Terzaghi's effective stress principle

$$\sigma_{ij} = \sigma'_{ij} + P\delta_{ij} \tag{6}$$

- Continuity equation including the compressibility of pore water

$$\frac{\partial \varepsilon_v}{\partial t} = -\frac{\partial q_i}{\partial x_i} + n'\beta\frac{\partial P}{\partial t} \tag{7}$$

The volumetric strain of soil skeleton is given as:

$$\varepsilon_v = \frac{\partial u_i}{\partial x_i} \tag{8}$$

where σ_{ij}, σ'_{ij} and P are total stress tensor, effective stress tensor and excess pore water pressure (pore water pressure is called later) at any time t and b_i the unit body force. Δu_i is the displacement increment and $\Delta\sigma_{ij}$, $\Delta\varepsilon_{ij}$ total stress and strain increments in time interval $[t, t+\Delta t]$. The discharge of excess pore water is q_i in the ith direction. γ_w is the density of water. In SI system, its value can be taken as 10 $\mathrm{kN/m^3}$. D_{ijkl} is the material matrix of soil skeleton determined by the constitutive law of materials. K_{ij} is a permeability tensor of soil skeleton which usually has non-zero components K_x in x direction and K_y in y direction, respectively. The porosity of the seabed is n' and the compressibility of the pore water is denoted as β.

2.1. For soil skeleton boundary

$$\begin{cases} u_i = \bar{u}_{i0} & \text{on } S_{\bar{u}} \times [0,\infty) \\ \sigma'_{ij}n_j = \bar{T}_i & \text{on } S_\sigma \times [0,\infty) \end{cases} \tag{9}$$

where $\mathbf{n} = \{n_1\ n_2\ n_3\}$ is the outward normal direction and n_i is its directional

cosine. The traction boundary and the essential boundary form conventional boundaries. A periodic boundary is additional to express the periodicity of the seabed response on virtual boundaries. The displacements of soil skeleton satisfy following periodicity on these virtual boundaries:

$$u_i(y+\mathbf{Y}) = u_i(y) \quad \text{on } S_Y \times [0,\infty) \tag{10}$$

Essential, traction and periodicity boundaries form complete boundaries of this problem. They have following relationship (Φ is an empty set):

$$S_{\bar{u}} \cup S_\sigma \cup S_Y = \Gamma \quad S_{\bar{u}} \cap S_\sigma = \Phi \quad S_{\bar{u}} \cap S_Y = \Phi \quad S_Y \cap S_\sigma = \Phi \tag{11}$$

2.2. For pore fluid boundary

$$\begin{cases} P = P_0 & \text{on } S_p \times [0,\infty) \\ q_i = q_{i0} & \text{on } S_q \times [0,\infty) \end{cases} \tag{12}$$

The pore water pressure P_0 at the interface (S_P) can be estimated through linear wave theory (Madsen, 1976). The bottom (S_q) is usually impervious ($q_{i0} = 0$). On the virtual boundaries (S_Y), the pore water pressure should satisfy periodicity boundary condition as:

$$P(y+\mathbf{Y}) = P(y) \qquad \text{on } S_Y \times [0,\infty) \tag{13}$$

2.3. Initial condition

$$\begin{cases} u_i = 0 \\ P = 0 \end{cases} \quad \text{on } \mathrm{V} \times 0^- \tag{14}$$

The variables within the time interval of $[t,\ t+\Delta t]$ are of interest. If one-step incremental approach is adopted in time domain, the variables are all known at time t. The displacement increments of soil skeleton satisfies the weak form of the equilibrium Eq. (2) as

$$\begin{aligned} &\int_V \{\delta(\Delta\varepsilon)\}^T\{\Delta\sigma'\}\mathrm{d}v + \int_V \left\{\delta\left(\frac{\partial \Delta u_i}{\partial x_i}\right)\right\}^T \{P\}^{t+\Delta t}\mathrm{d}v - \int_{S_\sigma} \{\delta(\Delta\bar{\boldsymbol{u}})\}^T\{n\}P^{t+\Delta t}\mathrm{d}s \\ &\quad - \int_{S_\sigma} \{\delta(\Delta\bar{\boldsymbol{u}})\}^T\{\Delta\bar{\boldsymbol{T}}\}\mathrm{d}s - \int_V \{\delta(\Delta\bar{\boldsymbol{u}})\}^T\{\Delta b\}\mathrm{d}v = -\int_V \{\delta(\Delta\varepsilon)\}^T\{\sigma' t\}\mathrm{d}v \\ &\quad + \int_{S_\sigma} \{\delta(\Delta\bar{\boldsymbol{u}})\}^T\{\bar{\boldsymbol{T}}\}^t\mathrm{d}v + \int_V \{\delta(\Delta\bar{\boldsymbol{u}})\}^T\{b^t\}\mathrm{d}v \end{aligned} \tag{15}$$

where $\delta(\Delta\bar{\boldsymbol{u}})$ is the variational of displacement increment. The "δ" denotes the variational. The term at the right hand side includes the un-balanced force at the previous time step. This un-balanced force can be automatically corrected in the next step. Thus Eq. (15) can prevent error from accumulation. This auto-corrector is especially useful in incremental computation schemes for dissipation problems.

The weak form of the continuity equation is obtained as follows:

$$\frac{1}{\gamma_w}\int_V \left\{\frac{\partial \delta P}{\partial x_i}\right\}^T \left\{K_i \frac{\partial P}{\partial x_i}\right\} \mathrm{d}v + \int_V \{\delta P\}^T \frac{\partial}{\partial t}\left\{\frac{\partial \Delta u_i}{\partial x_i}\right\} \mathrm{d}v - \int_V n'\beta \delta P \frac{\partial P}{\partial t}\mathrm{d}v - \frac{1}{\gamma_w}\int_{S_q} \{\delta P\}^T \{q\}\mathrm{d}s = 0 \quad (16)$$

where δP expresses the variational of the pore water pressure. Compared with our previous results (Wang et al., 2002), the periodicity condition does not modify the weak form.

3. Discretization of weak forms

A spatial discretization for displacement and pore water pressure is as follows:

$$\mathbf{u} = \sum_{i=1}^{n} N_i \mathbf{u}_i \quad P = \sum_{i=1}^{n} N_i P_i \quad (17)$$

where $\mathbf{u}_i$, P_i are nodal displacement and pore water pressure, respectively. The shape function N_i can be determined through either radial PIM (Wang and Liu, 2002a) or FEM (Sandhu and Wilson, 1969). Using the same shape functions for the pore water pressure and the displacement is effective to the solution of Biot's consolidation theory (Wang et al., 2002). After above approximation, the weak form of Eq.(15) is discretized as:

$$K\Delta\mathbf{u} + K_V\mathbf{P} = F_b + F_t + F_p \quad (18)$$

where

$$K = \int_V B^T D B \mathrm{d}v, \quad K_V = \int_V B_V^T N \mathrm{d}v, \quad F_b = \int_V N^T b \mathrm{d}v$$
$$F_t = \int_{S_\sigma} N^T T \mathrm{d}s, \qquad F_p = \int_{S_\sigma} N^T P \mathrm{d}s \quad (19)$$

For plane stress problem, the matrices $\mathbf{B}_i$, $\mathbf{D}$ are expressed as

$$\mathbf{B}_i = \begin{bmatrix} N_{i,x} & 0 \\ 0 & N_{i,y} \\ N_{i,y} & N_{i,x} \end{bmatrix}, \quad \mathbf{B}_{Vi} = \begin{bmatrix} N_{i,x} & 0 \\ 0 & N_{i,y} \end{bmatrix}, \quad \mathbf{D} = \frac{E}{1-v^2}\begin{bmatrix} 1 & v & 0 \\ v & 1 & 0 \\ 0 & 0 & (1-v)/2 \end{bmatrix} \quad (20)$$

where E, v are the Young's modulus and Poisson ratio, respectively.

After differentiating with time, above equation becomes

$$K\frac{\mathrm{d}\mathbf{u}}{\mathrm{d}t} + K_V\frac{\mathrm{d}\mathbf{P}}{\mathrm{d}t} = \frac{\mathrm{d}\left(F_b + F_t + F_p\right)}{\mathrm{d}t} \quad (21)$$

The continuity equation is discretized into

$$K_V^T \frac{\mathrm{d}\mathbf{u}}{\mathrm{d}t} - K_{pt} \frac{\mathrm{d}\mathbf{P}}{\mathrm{d}t} + K_p \mathbf{P} = F_q \tag{22}$$

where

$$K_p = \int_V B_p^T K B_p \mathrm{d}v, \quad K_{pt} = \int_V n' \beta N^T N \mathrm{d}v, \quad F_q = \int_{S_q} N^T q n \mathrm{d}s \tag{23}$$

and

$$K_i = \begin{bmatrix} K_x & 0 \\ 0 & K_y \end{bmatrix}, \quad \mathbf{B}_{Pi} = [\, N_{i,x} \quad N_{i,y} \,] \tag{24}$$

A single step method is applied to the time domain:

$$\int_t^{t+\Delta t} f(x)\mathrm{d}x = \Delta t[(1-\theta)f(t) + \theta f(t+\Delta t)] \tag{25}$$

A system equation for the wave-induced transient response problem is obtained as

$$\begin{bmatrix} K & K_V \\ K_V^T & (\Delta t \theta K_p - K_{pt}) \end{bmatrix} \begin{Bmatrix} \Delta \mathbf{u} \\ \Delta \mathbf{P} \end{Bmatrix} = \begin{bmatrix} 0 & 0 \\ 0 & -\Delta t K_p \end{bmatrix} \begin{Bmatrix} \mathbf{u}^t \\ \mathbf{P}^t \end{Bmatrix} + \begin{Bmatrix} \Delta F_b + \Delta F_t + \Delta F_p \\ \Delta t F_q \end{Bmatrix} \tag{26}$$

If the pore water pressure, $\mathbf{P}^{t+\Delta t} = \mathbf{P}^t + \Delta \mathbf{P}$, is used as unknowns, Eq. (26) can be rewritten as

$$\begin{bmatrix} K & K_V \\ K_V^T & (\Delta t \theta K_p - K_{pt}) \end{bmatrix} \begin{Bmatrix} \Delta \mathbf{u} \\ \mathbf{P}^{t+\Delta t} \end{Bmatrix} = \begin{Bmatrix} F_b^t + F_t^t + F_p^t + F_r^t \\ \Delta t F_q - [\Delta t(1-\theta)K_p + K_{pt}]\mathbf{P}^t \end{Bmatrix} \tag{27}$$

where

$$F_b^t = \int_V N^T \Delta b \mathrm{d}v, \qquad F_t^t = \int_{S_\sigma} N^T \Delta T \mathrm{d}s, \qquad F_p^t = \int_{S_\sigma} N^T P \mathrm{d}s$$
$$F_r^t = -\int_V B^T \sigma' t \mathrm{d}v + \int_{S_\sigma} N^T \bar{T}^t \mathrm{d}s + \int_V N^T b^t \mathrm{d}v \tag{28}$$

4. Numerical treatment for boundary conditions

4.1. Periodicity conditions

The periodicity conditions on the virtual boundary (S_Y) are

$$\mathbf{u}_i(y) = \mathbf{u}_i(y + \mathbf{Y}), \qquad P(y) = P(y + \mathbf{Y}) \tag{29}$$

Above periodicity conditions can be easily implemented in the assembling process of the system equation. This is because the interpolation of the radial PIM passes

through each node point within an influence domain. Before the introduction of periodicity conditions, the discretized system equation is obtained as:

$$K_{ir}U_r = F_i \qquad \text{where} \qquad r, i = 1, 2, \ldots, m \tag{30}$$

The periodicity conditions impose following constraint along virtual boundaries:

$$U_j = U_k \tag{31}$$

If the Eq. (31) is introduced into Eq. (30), the final system equation reduces its size as

$$\begin{cases} \underbrace{K_{ir}U_r}_{r\neq j,k} + \left(K_{ik} + K_{ij}\right)U_k = F_i & i \neq k \\ \underbrace{\left(K_{kr} + K_{jr}\right)U_r}_{r\neq j,k} + \left(K_{kk} + 2K_{kj} + K_{jj}\right)U_k = F_k + F_j & i = k \end{cases} \tag{32}$$

It is noted that the unknown U_j has been eliminated from the system equation. This approach can be implemented on either global or local level. The implementation at global level is completed according to following steps: assembling system equation without periodicity conditions, introducing periodicity conditions with the help of Eq. (32). Such an approach has two disadvantages: system stiffness equation will reduce its size after implementing periodicity conditions. Because the global system stiffness must be stored, the size reduction may waste some storage space. Furthermore, because the operation is carried out in the global system stiffness, computational efficiency is not high. These two disadvantages can be overcome through the implementation at local level. The system stiffness is assembled by the local stiffness at each Gaussian point. If a periodic pair of nodes is assigned to the same equation number, the revised stiffness equation from the periodicity conditions is automatically assembled at each Gaussian point.

4.2. Wave load at the interface of fluid and seabed

The interface condition for a two-dimensional wave-induced problem is given as follows:

$$\sigma'_y = 0 \quad \tau_{xy} = 0 \quad P = P_0\cos(ax - \omega t) \tag{33}$$

where the maximum water pressure (P_0) can be determined through linear wave theory (Madsen, 1976) as

$$P_0 = \frac{\gamma_w H}{2\cosh(ad)} \tag{34}$$

where H is the wave height, d the static water depth and a the wave number which is determined through wavelength (L) and period (T). ω is the angular velocity. Above essential boundary conditions can also be implemented at local level. After

introduction of periodicity conditions, the system equation is expressed as follows:

$$K_{ir}U_r = F_i \qquad \text{where} \qquad r, i = 1, 2, \ldots, n \tag{35}$$

with the constraint from the essential condition

$$U_j = b \tag{36}$$

After introducing the Eq. (35) into Eq. (36), the final system equation is obtained as

$$K_{ir}U_r = F_i - bK_{kj} \qquad r \neq j \tag{37}$$

5. Radial point interpolation method

5.1. Radial PIM for two-dimensional problems

Consider an approximation function $u(\mathbf{x})$ in any influence domain that has arbitrarily distributed points $P_i(\mathbf{x}_i)$ $(i = 1, 2, \ldots, n)$ with the function value u_i. The $u(\mathbf{x})$ can be expressed by radial basis $B_i(\mathbf{x})$ and polynomial basis $p_j(\mathbf{x})$:

$$u(\mathbf{x}) = \sum_{i=1}^{n} B_i(\mathbf{x})a_i + \sum_{j=1}^{m} P_j(\mathbf{x})b_j = \mathbf{B}^{\mathrm{T}}(\mathbf{x})\mathbf{a} + \mathbf{P}^{\mathrm{T}}(\mathbf{x})\mathbf{b} \tag{38}$$

where a_i is the coefficient for $B_i(\mathbf{x})$ and b_j the coefficient for $p_i(\mathbf{x})$ (usually $m < n$). The vectors are defined as

$$\begin{aligned}
&\mathbf{a}^T = [\,a_1 \quad a_2 \quad a_3 \quad \cdots \quad a_n\,] \\
&\mathbf{b}^T = [\,b_1 \quad b_2 \quad \cdots \quad b_m\,] \\
&\mathbf{B}^T(\mathbf{x}) = [\,B_1(\mathbf{x}) \quad B_2(\mathbf{x}) \quad B_3(\mathbf{x}) \quad \cdots \quad B_n(\mathbf{x})\,] \\
&\mathbf{P}^T(\mathbf{x}) = [\,p_1(\mathbf{x}) \quad p_2(\mathbf{x}) \quad \cdots \quad p_m(\mathbf{x})\,]
\end{aligned} \tag{39}$$

Generally, the $B_i(\mathbf{x})$ has following form for a two-dimensional problem

$$B_i(\mathbf{x}) = B_i(r_i) = B_i(x, y) \tag{40}$$

where r_i is a distance between interpolating point (x, y) and node (x_i, y_i) defined as

$$r_i = \left[(x - x_i)^2 + (y - y_i)^2\right]^{1/2} \tag{41}$$

Polynomial basis functions have monomial terms:

$$\mathbf{P}^T(\mathbf{x}) = \begin{bmatrix} 1 & x & y & x^2 & xy & y^2 & \cdots \end{bmatrix} \tag{42}$$

The coefficients a_i and b_j in Eq. (38) are determined by enforcing the $u(\mathbf{x})$ to pass through all n scattered points. For example, the interpolation at the kth point has

$$u_k = u(x_k, y_k) = \sum_{i=1}^{n} a_i B_i(x_k, y_k) + \sum_{j=1}^{m} b_j P_j(x_k, y_k) \qquad k = 1, 2, \ldots, n \tag{43}$$

A constraint is imposed to guarantee the uniqueness of the interpolation:

$$\sum_{i=1}^{n} P_j(x_i, y_i) a_i = 0 \qquad j = 1, 2, \ldots, m \tag{44}$$

It is expressed in matrix form as follows

$$\begin{bmatrix} \mathbf{B_0} & \mathbf{P}_0 \\ \mathbf{P}_0^T & \mathbf{0} \end{bmatrix} \begin{Bmatrix} \mathbf{a} \\ \mathbf{b} \end{Bmatrix} = \begin{Bmatrix} \mathbf{u}^e \\ \mathbf{0} \end{Bmatrix} \quad \text{or} \quad \mathbf{G} \begin{Bmatrix} \mathbf{a} \\ \mathbf{b} \end{Bmatrix} = \begin{Bmatrix} \mathbf{u}^e \\ \mathbf{0} \end{Bmatrix} \tag{45}$$

where the vector for function values at each node is

$$\mathbf{u}^e = [\, u_1 \quad u_2 \quad u_3 \quad \cdots \quad u_n \,]^T \tag{46}$$

The coefficient matrix $\mathbf{B}_0$ on unknowns $\mathbf{a}$ is

$$\mathbf{B_0} = \begin{bmatrix} B_1(x_1, y_1) & B_2(x_1, y_1) & \cdots & B_n(x_1, y_1) \\ B_1(x_2, y_2) & B_2(x_2, y_2) & \cdots & B_n(x_2, y_2) \\ \vdots & \vdots & \vdots & \vdots \\ B_1(x_n, y_n) & B_2(x_n, y_n) & \cdots & B_n(x_n, y_n) \end{bmatrix}_{n \times n} \tag{47}$$

The coefficient matrix $\mathbf{P}_0$ on unknowns $\mathbf{b}$ is

$$\mathbf{P_0} = \begin{bmatrix} P_1(x_1, y_1) & P_2(x_1, y_1) & \cdots & P_m(x_1, y_1) \\ P_1(x_2, y_2) & P_2(x_2, y_2) & \cdots & P_m(x_2, y_2) \\ \vdots & \vdots & \vdots & \vdots \\ P_1(x_n, y_n) & P_2(x_n, y_n) & \cdots & P_m(x_n, y_n) \end{bmatrix}_{n \times m} \tag{48}$$

The distance is directionless, $B_k(x_i, y_i) = B_i(x_k, y_k)$. The unique solution is obtained if the inverse of matrix $\mathbf{G}$ or $\mathbf{B}_0$ exists:

$$\begin{Bmatrix} \mathbf{a} \\ \mathbf{b} \end{Bmatrix} = \mathbf{G}^{-1} \begin{Bmatrix} \mathbf{u}^e \\ \mathbf{0} \end{Bmatrix} \tag{49}$$

The interpolation is finally expressed as

$$u(\mathbf{x}) = \begin{bmatrix} \mathbf{B}^T(\mathbf{x}) & \mathbf{P}^T(\mathbf{x}) \end{bmatrix} \mathbf{G}^{-1} \begin{Bmatrix} \mathbf{u}^e \\ \mathbf{0} \end{Bmatrix} = \mathbf{N}(\mathbf{x}) \mathbf{u}^e \tag{50}$$

where the matrix of shape functions $\mathbf{N}(\mathbf{x})$ is defined by

$$\begin{aligned} &\mathbf{N}(\mathbf{x}) = [\, N_1(\mathbf{x}) \quad N_2(\mathbf{x}) \quad \cdots \quad N_i(\mathbf{x}) \quad \cdots \quad N_n(\mathbf{x}) \,] \\ &N_k(\mathbf{x}) = \sum_{i=1}^{n} B_i(\mathbf{x}) \bar{G}_{i,k} + \sum_{j=1}^{m} P_j(\mathbf{x}) \bar{G}_{n+j,k} \end{aligned} \tag{51}$$

where $\bar{G}_{i,k}$ is the (i,k) element of matrix $\mathbf{G}^{-1}$. Once the inverse of matrix $\mathbf{G}$ is

obtained, the derivatives of shape functions are

$$\begin{aligned}\frac{\partial N_k}{\partial x} &= \sum_{i=1}^{n} \frac{\partial B_i}{\partial x} \bar{G}_{i,k} + \sum_{j=1}^{m} \frac{\partial P_j}{\partial x} \bar{G}_{n+j,k} \\ \frac{\partial N_k}{\partial y} &= \sum_{i=1}^{n} \frac{\partial B_i}{\partial y} \bar{G}_{i,k} + \sum_{j=1}^{m} \frac{\partial P_j}{\partial y} \bar{G}_{n+j,k}\end{aligned} \tag{52}$$

5.2. Radial basis function

The $B_i(x, y)$ can be taken as a compactly supported basis function which has a general form as follows:

$$B_i(r) = B_i(x,\ y) = c(\bar{r})S(\bar{r}) \qquad \bar{r} = \frac{r_i}{r_{\max}} \tag{53}$$

where $c(\bar{r})$ is a compactly supported function and $S(\bar{r})$ is a radial basis function which has sufficient smoothness. $r_{\max}$ is the radius of the influence domain. A compactly supported function should be zero out of an influence domain or local non-zero. Two types of compactly supported parts are tested in this paper. The first one is taken as following jump form:

$$c(\bar{r}) = \begin{cases} 1 & \bar{r} \le 1 \\ 0 & \bar{r} > 1 \end{cases} \tag{54}$$

This type includes extended multiquadric basis (called MQ by Hardy (1990)) which has following form:

$$B_i(x,\ y) = \left(r_i^2 + R^2\right)^q \quad R \ge 0 \tag{55}$$

where q and R are two shape parameters. The partial derivatives are obtained as follows

$$\begin{aligned}\frac{\partial B_i}{\partial x} &= 2q\left(r_i^2 + R^2\right)^{q-1}(x - x_i) \\ \frac{\partial B_i}{\partial y} &= 2q\left(r_i^2 + R^2\right)^{q-1}(y - y_i)\end{aligned} \tag{56}$$

Furthermore, a quartic spline can also be used as radial basis function:

$$B_i(\bar{r}) = 1 - 6\bar{r}^2 + 8\bar{r}^3 - 3\bar{r}^4 \quad \text{denoted by Quart} \tag{57}$$

And their derivatives are

$$\begin{aligned}\frac{\partial B_i}{\partial x} &= \left(-12\bar{r} + 24\bar{r}^2 - 12\bar{r}^3\right)\frac{x - x_i}{r_{\max} r_i} \\ \frac{\partial B_i}{\partial y} &= \left(-12\bar{r} + 24\bar{r}^2 - 12\bar{r}^3\right)\frac{y - y_i}{r_{\max} r_i}\end{aligned} \tag{58}$$

The compactly supported part can also be taken following smooth function as

$$c(\bar{r}) = \begin{cases} (1-\bar{r})^m & \bar{r} \le 1 \\ 0 & \bar{r} > 1 \end{cases} \tag{59}$$

where m is a parameter whose performance can be observed in Fig. 2. When $\bar{r}$ approaches to one, the function and its derivative all approach to zero. The $S(\bar{r})$ is usually taken as polynomial. Therefore, their derivatives are as follows:

$$\begin{aligned} \frac{\partial B_i}{\partial x} &= \left[m(1-\bar{r})^{m-1} S(\bar{r}) + (1-\bar{r})^m \frac{\mathrm{d}S(\bar{r})}{\mathrm{d}\bar{r}} \right] \frac{x - x_i}{r_{\max} r_i} \\ \frac{\partial B_i}{\partial y} &= \left[m(1-\bar{r})^{m-1} S(\bar{r}) + (1-\bar{r})^m \frac{\mathrm{d}S(\bar{r})}{\mathrm{d}\bar{r}} \right] \frac{y - y_i}{r_{\max} r_i} \end{aligned} \tag{60}$$

Wendland (1995) proposed a class of compactly supported RBFs which are strictly positive definite in $\mathbb{R}^d$ for all d. They can achieve any desired amount of smoothness 2κ. This paper lists two typical basis functions as follows:

$$\begin{aligned} B_i(\bar{r}) &= (1-\bar{r})^4 (4\bar{r}+1) && \text{denoted by CSF1} \\ B_i(\bar{r}) &= (1-\bar{r})^4 \left(4 + 16\bar{r} + 12\bar{r}^2 + 3\bar{r}^3\right) && \text{denoted by CSF2} \end{aligned} \tag{61}$$

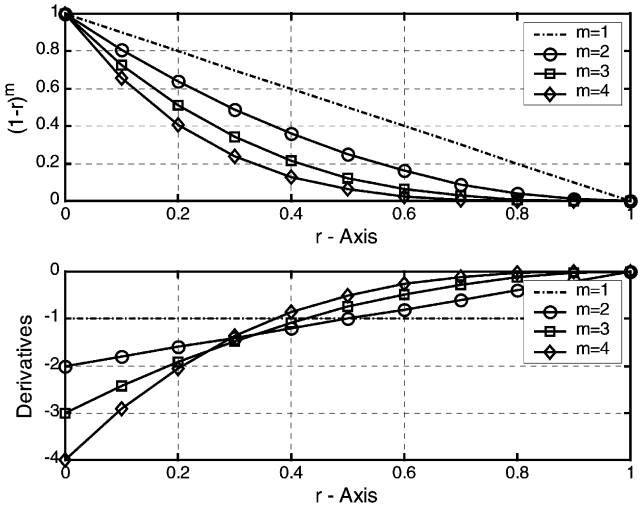

Fig. 2. Compactly supported functions with different parameter m.

6. Assessment through numerical examples

6.1. Transient response of the seabed under progressive wave

Fig. 3 shows the meshless models for a 10 m thick seabed. Irregular and regular distributions of nodes are shown in Fig. 3(a), (b), respectively. The bottom is fixed for displacements and impervious for the pore water pressure. Both side virtual boundaries are periodic. Either the displacement or the pore water pressure is identical at the same depth and the same time. The upper boundary has the wave-induced water pressure. The seabed soil mass is linearly elastic with Young's modulus $E = 40\ 000.0$ kPa and Poisson ratio $v = 0.3$. The permeability is assumed to be isotropic with $k_x = k_y = 1.728 \times 10^{-3}$ m/s. The pore fluid is assumed to be incompressible in the current computation. Wave parameters in the computation are as follows: water depth is 5 m, wave height is 0.5 m and wave period is 5 s. For such a wave, the wavelength is approximately 30 m, thus the meshless model is taken as 30 m long which is one wavelength. This computational domain (30 m long and 10 m deep) is discretized with irregular and regular distribution of nodes as shown in Fig. 3(a), (b). They have 246 and 341 nodes, respectively. In the MQ basis function, the shape parameters are taken as $q = 1.03$ and $R = 0.1$ (Wang et al., 2002). Time domain employs fully implicit scheme ($\theta = 1$) to avoid the spurious ripple effect. Time step size is taken as 0.001 s for the first step and 0.05 s for the subsequent steps. Total 30 s are computed.

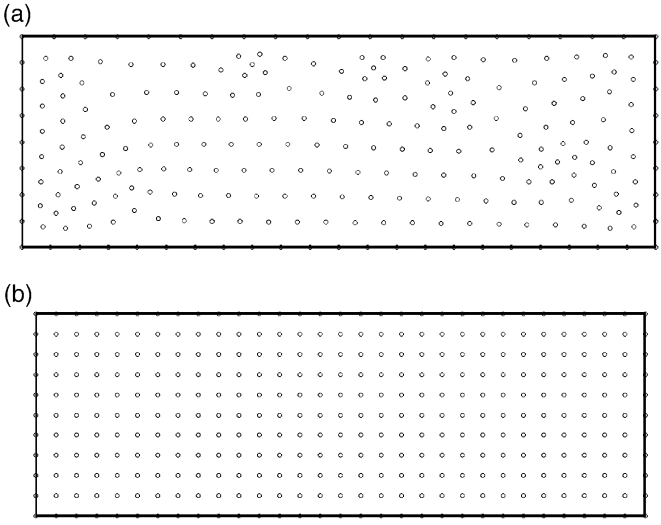

Fig. 3. Meshless models with regular and irregular nodal distributions.

6.2. Comparison with Madsen's and Hsu and Jeng's solutions

Madsen's solution (1978) and Hsu and Jeng's closed-form solution (1994) are two typical solutions for the wave-induced transient responses of the seabed. For the seabed with infinite thickness, Madsen developed a closed-from solution for the pore water pressure as follows:

$$\frac{P}{P_0} = \text{real}\left\{\left(-C_6\, e^{k_* kz} + C_7\, e^{kz}\right) e^{i(kx-\omega t)}\right\} \tag{62}$$

where k_* is a parameter associated with anisotropic permeability. When soil mass is isotropic in permeability, the $k_* = 1$. C_6, C_7 are constants associated with Poisson ratio, anisotropy of permeability, and compressibility of pore water.

For the seabed with finite thickness, Hsu and Jeng (1994) developed a closed-form solution for the pore water pressure in complex space:

$$P = \frac{P_0}{(1-2\mu)}\left\{(1-\lambda-2\mu)\left(C_2\, e^{kz} - C_4\, e^{-kz}\right) + (1-\mu)\left(\delta^2 - k^2\right)\left(C_5\, e^{\delta z} + C_6\, e^{-\delta z}\right)\right\} e^{i(kx-\omega t)} \tag{63}$$

The real part is the excess pore water pressure. Where λ, δ, μ are material constants. The coefficients $C_2 - C_6$ are determined from the material constants.

The results on history curves are compared for above problem. Fig. 4 compares typical history curve of pore water pressure at a point near seabed surface. The numerical results agree well with closed-form solutions. As pointed out in previous section, the Madsen's solution was obtained for infinite soil layer, thus they have a little difference for finite thickness case, especially at the location near bottom. Fig. 5

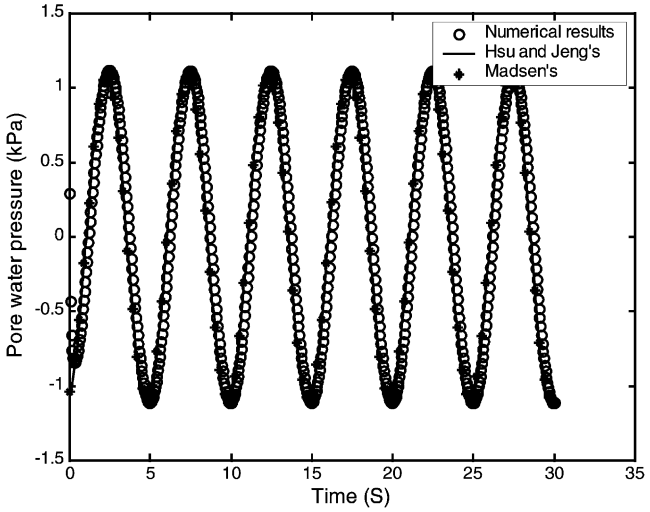

Fig. 4. Comparison of numerical results with closed-form solutions.

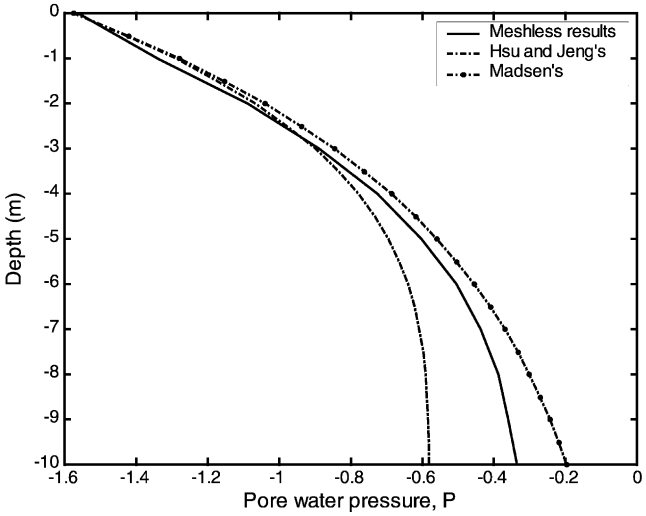

Fig. 5. Sectional comparison for numerical results and closed-form solutions.

shows this difference which is a sectional distribution of excess pore water pressure at time $t = 9.80$ s. This result is obtained for the regular distribution of nodes as shown in Fig. 3(b). FEM results with four-node isoparametric element are also presented for comparison as shown in Fig. 6. The meshless method agrees very well with the FEM. It approaches to the Madsen's solution and Hsu and Jeng's solution. If the detail at the bottom is observed, the meshless and FEM results are closer to the Madsen's solution. As a summary, the current meshless model can give reasonable numerical results for a finite thickness problem.

7. Parameter study

7.1. Effect of influence domain size

Influence domain size is an important parameter in meshless methods. It will affect the numerical accuracy and computational efficiency. Larger domain size has wider bandwidth of the system equation, thus spending more CPU time. On the other hand, accuracy cannot be guaranteed for too small domain size. Radial basis functions have less imposition on the node distribution within an influence domain. However, polynomial basis function has a minimum requirement for the node number. For example, linear polynomial basis requires minimum nodes in an influence domain at least more than 3. If a prescribed influence domain embraces less than three nodes, the domain size should be enlarged until the minimum nodes are embraced. For computational consideration, a maximum of nodes within an influence domain is set to 30. If the nodes within the prescribed influence domain are

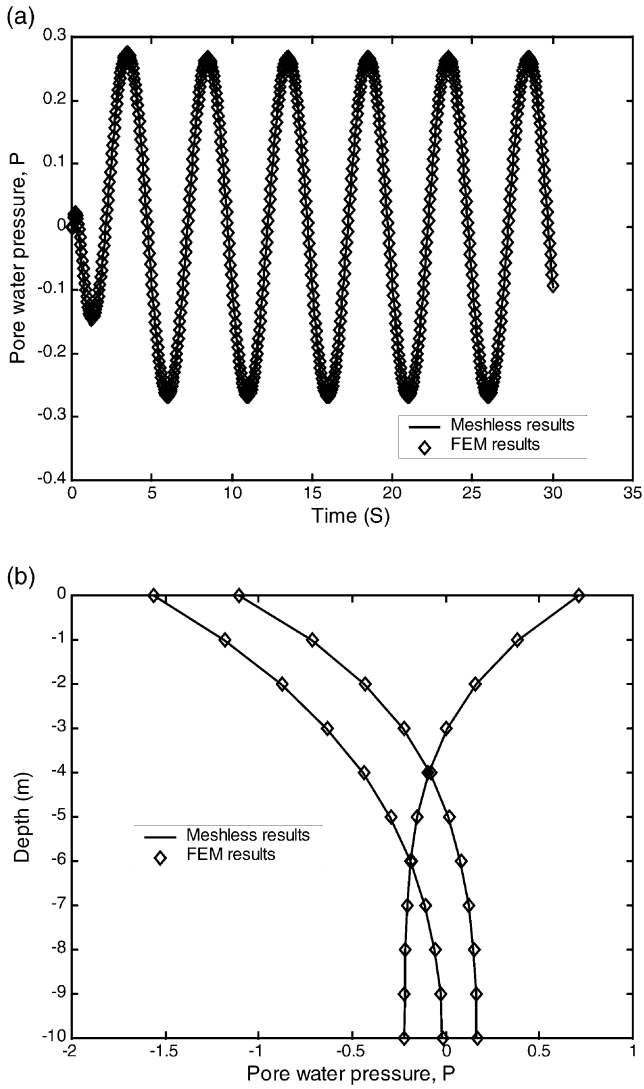

Fig. 6. Comparison of numerical results obtained by meshless method and FEM.

more than the maximum, only nearest 30 nodes are taken for interpolation. In this computation, influence domain sizes vary from 1.2, 1.5, 1.7 and 2.0. The average nodes embraced in each influence domain are 6.15, 6.56, 8.57 and 11.22, respectively.

Fig. 7 compares numerical results for different influence domain sizes. This computation is completed for the MQ basis function. The time step size is fixed at 0.2 s. Fig. 7(a) shows the pore water pressure on the seabed interface. According to

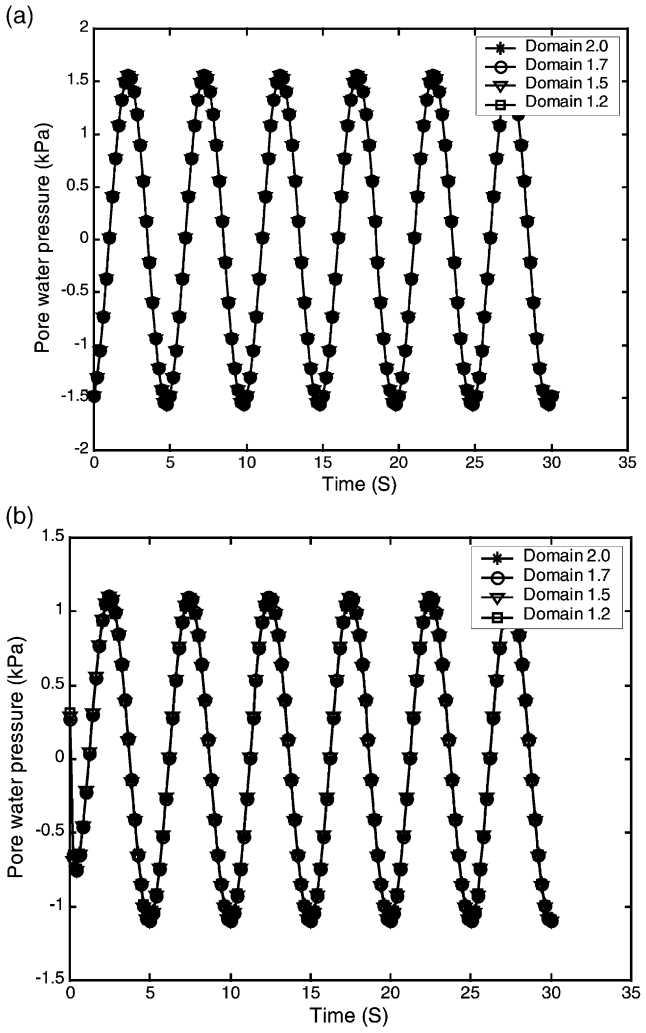

Fig. 7. Effect of influence domain size on the numerical results.

boundary conditions, the pore water pressure should be the same as wave-induced water pressure. As shown in Fig. 7(a), all numerical results are indeed the same for different influence domain sizes. The pore water pressures are little different for internal points. A typical example is shown in Fig. 7(b). However, even if the influence domain varies within a big range, numerical results are almost the same. In other words, numerical results are not sensitive to influence domain sizes. Domain size of 1.5 is a good choice.

7.2. Effect of time step size

Time step size is a vital parameter to affect the accuracy and efficiency of the current algorithm. For the irregular distribution of nodes, the time step sizes are taken from 0.05 to 0.5 s to study the effect of time step sizes. A typical numerical result is shown in Fig. 8 for the point (13.82, 8.69). Fig. 8(a) expresses the whole history of the pore water pressure at this point. The numerical results are in general not sensitive to time step size. However, large time step size cannot capture the peak of the pore water pressure as shown in Fig. 8(b). This is because the pore

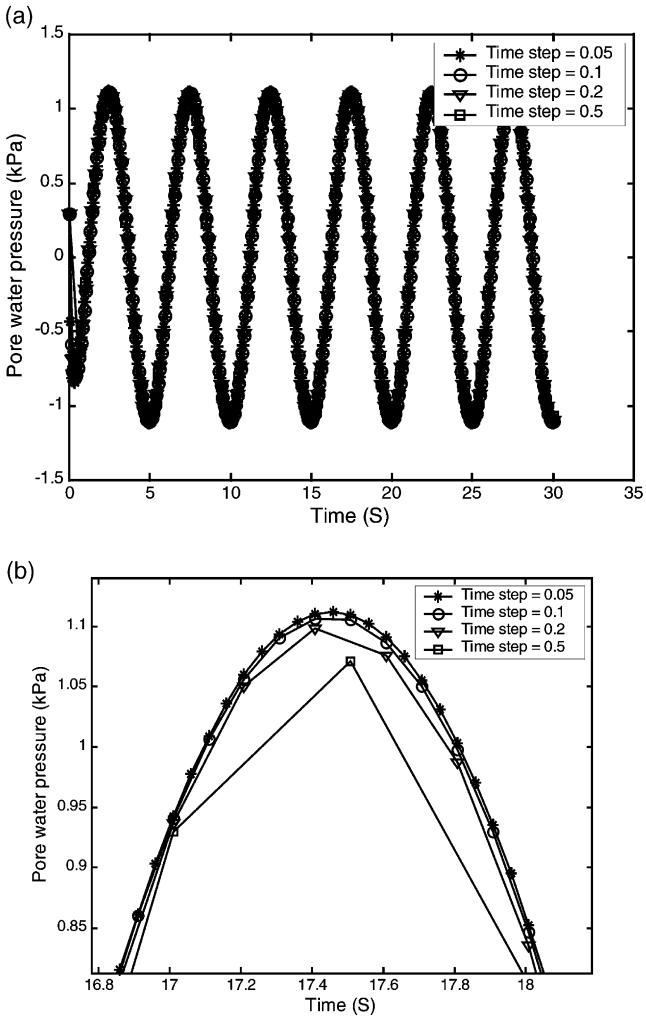

Fig. 8. Effect of time step size on the numerical results.

water pressure changes drastically at the peak. Smaller time step size is required in this range. Detailed analysis shows that 100 time steps per period are sufficient to capture the peak properties of pore water pressure as shown in Fig. 8(b).

7.3. Effect of radial basis functions

The accuracy of the current algorithm is controlled by two factors: weak form and basis function. This section compares the numerical results obtained by the different radial basis functions of MQ, CSF1, CSF2 and Quart. When the irregular distribution of nodes as shown in Fig. 3(a) is used, the maximum pore water pressures at the node 112 are compared in Table 1. Fig. 9 shows typical comparison of the pore water pressure at node point 114, which is near the bottom. The FEM results are also presented for comparison. From these results, we can observe following findings: firstly, the numerical results obtained by MQ and Quart agree well with FEM results. If the FEM is used as a standard, MQ and Quart have better results than CSF1 and CSF2 whether polynomial terms are included or not. The MQ has the best accuracy for the current shape parameters. Secondly, linear polynomial included does not always improve the accuracy of the radial PIM. The polynomial can improve the accuracy for MQ and Quart, but worsen the accuracy for CSF1 and CSF2. Thirdly, different compactly supported part has a vital effect on the accuracy of the current algorithm. For example, we once try to apply the smooth compactly supported part to Quart, the numerical results are not acceptable.

8. Conclusions

The wave-induced transient response of the seabed is numerically analyzed through a radial PIM with compactly supported basis functions. Basis functions include both polynomial and radial basis functions. In the current algorithm, spatial variables, displacement increment and pore water pressure, are all discretized by the same shape function constructed by radial PIM. The discretization of time domain employs fully implicit scheme to eliminate spurious ripple effect. Numerical examples are compared with closed-form solutions and FEM results. Key parameters are studied to check its feasibility and effectiveness. From these studies, following conclusions can be drawn.

First, the radial point interpolation method is an effective interpolation technique for scattered node distributions. It is suitable not only for structured but also for unstructured nodes without singularity problem. This is its advantage over the

Table 1
Pore water pressures (kPa) at node No. 112

Polynomials (m)	MQ	CSF1	CSF2	Quart
0	1.096	1.074	1.118	1.119
3	1.107	0.927	0.959	1.135

The FEM result is 1.109 kPa.

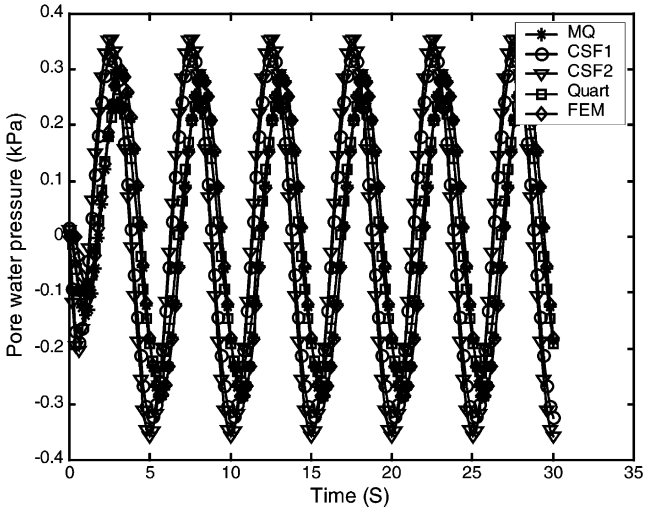

Fig. 9. Comparison of numerical results for different basis functions.

interpolation with only polynomial basis. Unlike those meshless methods based on the MLS method, the radial PIM method obtains its shape function and derivatives at the same time. The shape functions are of delta function properties, thus essential boundary conditions and virtual boundary conditions are easily implemented at either local or global level. This can largely improve the computational efficiency, especially for the wave-induced transient response of the seabed.

Second, influence domain size for the current algorithm is not sensitive to numerical results within some range. Our example shows that the influence domain can vary from 1.2 to 2.0 and an operational influence domain size of 1.5 is recommended. Minimum nodes within an influence domain depend on the order of polynomial and radial basis functions. This minimum node number should be more than the terms of polynomial basis. In our current examples, because linear polynomials are used, average nodes for each influence domain are more than 6.

Third, the current algorithm is efficient in time integration. Our example shows that the time step size can vary from 0.05 to 0.5 s, the numerical results agree well except the wave peak. In order to capture the wave peak value, 100 time steps per period are sufficient.

Fourth, different radial basis functions require different compactly supported parts and polynomials. The MQ and Quart require the jump type of compactly support part and linear polynomial to improve their accuracy, while CSF1 and CSF2 require the smooth type of compactly supported part and no polynomial. If the FEM is regarded as a standard, the MQ and Quart achieve better responses while CSF1 and CSF2 cannot achieve good responses for the current numerical examples. Furthermore, the polynomial term in basis functions can improve the

accuracy for MQ and Quart basis functions, but worsens the accuracy for CSF1 and CSF2 basis functions.

References

Belytschko, T., Krongauz, Y., Organ, D., Fleming, M., Krysl, P., 1996. Meshless methods: an overview and recent developments. Comput. Methods Appl. Mech. Eng. 139, 3–47.

Biot, M.A., 1941. General theory of three-dimensional consolidation. J. Appl. Phys. 12, 155–164.

Fasshauer, G.E., 1997. Solving partial differential equations by collocation with radial basis functions. In: Mehaute, A.L., Rabut, C., Schumaker, L.L. (Eds.), Surface Fitting and Multiresolution Methods. Vanderbilt University Press, Nashville, TN, pp. 131–138.

Hardy, R.L., 1990. Theory and applications of the multiquadrics—biharmonic method (20 years of discovery). Comput. Math. Appl. 19, 163–208.

Hsu, J.R.C., Jeng, D.S., 1994. Wave-induced soil response in an unsaturated anisotropic seabed of finite thickness. Int. J. Numer. Anal. Methods Geomech. 18, 785–807.

Jeng, D.S., Lin, Y.S., 1996. Finite element modeling for water waves–soil interaction. Soil Dyn. Earthquake Eng. 15 (5), 283–300.

Kansa, E.J., 1990. A scattered data approximation scheme with application to computational fluid-dynamics-I and II. Comput. Math. Appl. 19, 127–161.

Karim, M.R., Nogami, T., Wang, J.G., 2002. Analysis of transient response of saturated porous elastic soil under cyclic loading using element-free Galerkin method. Int. J. Solids Struct. 39 (6), 6011–6033.

Mase, H., Sakai, T., Sakamoto, M., 1994. Wave-induced pore water pressures and effective stresses around breakwater. Ocean Eng. 21 (4), 361–379.

Madsen, O.S., 1976. Wave climate of the continental margin: elements of its mathematical description. In: Stanley, D.F., Swift, D.J.P. (Eds.), Marine Sediment Transport and Environmental Management. John Wiley, New York, pp. 65–90.

Madsen, O.S., 1978. Wave-induced pore pressure and effective stresses in a porous bed. Geotechnique 28 (4), 377–393.

Modaressi, H., Aubert, P., 1998. Element-free Galerkin method for deforming multiphase porous media. Int. J. Numer. Methods Eng. 42, 313–340.

Liew, W.K., Jun, S., Zhang, Y.E., 1995. Reproducing kernel particle methods. Int. J. Numer. Methods Fluids 20, 1081–1106.

Liew, K.M., Wu, Y.C., Zou, G.P., Ng, T.Y., 2002. Elasto-plasticity revisited: numerical analysis via reproducing kernel particle method and parametric quadratic programming. Int. J. Numer. Methods Eng. 55, 669–683.

Okusa, S., 1985. Wave-induced stress in unsaturated submarine sediments. Geotechnique 35 (4), 517–532.

Sakai, T., Hatanaka, K., Mase, H., 1992. Wave-induced effective stress in seabed and its momentary liquefaction. J. Waterway Port Coast. Ocean Eng. 118 (2), 202–206.

Sandhu, R.S., Wilson, E.L., 1969. Finite element analysis of seepage in elastic media. J. Eng. Mech. Div., ASCE Proc. EM3, 641.

Sumer, B.M., Whitehouse, J.S., Torum, A., 2001. Scour around coastal structures: a summary of recent research. Coast. Eng. 44, 153–190.

Wang, J.G., Liu, G.R., 2002a. A point interpolation meshless method based on radial basis functions. Int. J. Numer. Methods Eng. 54 (11), 1623–1648.

Wang, J.G., Liu, G.R., 2002b. On the optimal shape parameters of radial basis functions used for 2-D meshless methods. Comput. Methods Appl. Mech. Eng. 191 (23-24), 2611–2630.

Wang, J.G., Liu, G.R., Lin, P., 2002. Numerical analysis of Biot's consolidation process by radial point interpolation method. Int. J. Solids Struct. 39 (6), 1557–1573.

Wendland, H., 1995. Piecewise polynomial, positive definite and compactly supported radial basis functions of minimal degree. Adv. Comput. Math. 4, 389–396.

Xie, H., Nogami, T., Wang, J.G., 2003. A radial boundary node method for two-dimensional elastic analysis. Eng. Anal. Boundary Elements 27 (8), 853–862.